High-energy-resolution XANES of layered oxides for sodium-ion battery

著者（英）	Hideharu NIWA, Kazuyuki HIGASHIYAMA, Kaoru Amaha, Wataru KOBAYASHI, Kenji Ishii, Yutaka MORITOMO
journal or publication title	Applied physics express
volume	12
number	5
page range	052005
year	2019-04
権利	(C)2019 The Japan Society of Applied Physics
URL	http://hdl.handle.net/2241/00159016

doi: 10.7567/1882-0786/ab10cd

High energy-resolved XANES of layered oxides for sodium-ion battery

Hideharu Niwa[1-3]*, Kazuyuki Higashiyama[1,2], Kaoru Amaha[1], Wataru Kobayashi[1-3], Kenji Ishii[4], Yutaka Moritomo[1-3]*

[1]*Graduate School of Pure and Applied Sciences, University of Tsukuba, Tsukuba 305-8571, Japan*

[2]*Faculty of Pure and Applied Sciences, University of Tsukuba, Tsukuba 305-8571, Japan*

[3]*Tsukuba Research Center for Energy Materials Science (TREMS), University of Tsukuba, Tsukuba 305-8571, Japan*

[4]*Synchrotron Radiation Research Center, National Institutes for Quantum and Radiological Science and Technology, Hyogo 679-5148, Japan*

E-mail: niwa.hideharu.ga@u.tsukuba.ac.jp, moritomo.yutaka.gf@u.tsukuba.ac.jp

Abstract

The 3*d* transition metal (TM) oxides with layered structure, Na_xMO_2 (*M* = Mn, Co), are promising cathode materials of sodium ion secondary batteries (SIBs). Here, we investigated the electronic structure of *M* of four layered oxides ($Na_{0.91}CoO_2$, $Na_{0.66}CoO_2$, $Na_{1.00}MnO_2$, and $Na_{0.54}MnO_2$) by means of high energy resolution fluorescence detected X-ray absorption near edge structure (HERFD-XANES), which utilizes the 1*s* core-hole lifetime-broadening-reduction. The high energy-resolved spectroscopy revealed a shoulder structure in the pre-edge regions of the Co K-edge spectra in $Na_{0.91}CoO_2$. The structure is ascribed to the transition to the Co 3*d*/4*p* state via slight hybridization with the Na 3*s* state.

X-ray absorption fine structure (XAFS) is widely used to evaluate the local structure and electronic states of material sciences.[1-3] In particular, X-ray absorption near edge structure (XANES) regions provides chemical information of materials such as oxidation states of metal compounds. Although XANES recorded with transmission mode or total fluorescence mode is very convenience for material science, the energy resolution is not necessarily sufficient to discuss the *d*-electron configuration. Recently, high energy resolution fluorescence detected XANES (HERFD-XANES) is receiving much attentions because it revealed detailed electronic structure[4-6] that cannot be detected by conventional XANES. For example, the energy resolution of the Pt L_3-edge XANES spectrum improved by HERFD-XANES from 5.2 eV to 2.4 eV due to a core-hole lifetime-broadening-reduction. The improved energy resolution clarified fine structures in the Pt L_3-edge spectrum of the Pt nanoparticle catalysts in the polymer electrolyte fuel cells, which suggests that surface hydrated species increase the overpotential, and hence, decrease the energy conversion efficiency. [4]

Figure 1(a) shows schematic diagram of X-ray absorption and fluorescence processes at the transition metal (TM) K-edge. The X-ray absorption and fluorescence processes contribute to the transmission XANES and HERFD-XANES, respectively. In the case of the transmission XANES, the lifetime of the absorption process from the 1*s*-core to the 4*s* (or 3*d*) levels is very short, and hence, causes the low energy resolution of the spectroscopy. For example, the spectral width (1*s*-core-hole lifetime width Γ_K) for Mn and Co is 1.16 and 1.33 eV, respectively.[7] On the other hand, the effective lifetime width of the HERFD-XANES (Γ) is given by

$$\Gamma = 1/\sqrt{\left(1/{\Gamma_K}^2\right) + \left(1/{\Gamma_M}^2\right)}, \quad (1)$$

where Γ_M is 3*p*-core-hole lifetime width.[8] The lifetime of the fluorescence process from the 3*p*-core to 1*s*-core levels is rather long, and hence, Γ is mainly determined by Γ_M. In other words, the HERFD-XANES used Γ_M instead of Γ_K to improve the energy resolution of the spectra. In the actual measurement of the HERFD-XANES, the detection energy of the scattered X-ray is fixed at the $K_{\beta_{1,3}}$ fluorescence line while the energy of the incident X-ray is scanned over the absorption edge [Fig. 1(b)].

Sodium ion secondary batteries (SIBs) have attracted much attention as promising candidates for next-generation batteries beyond lithium ion secondary batteries.[9-12] Among

several types of cathode materials for SIBs, layered transition metal oxides Na_xMO_2(M = Co, Mn) are the most typical and promising cathode materials.[13,14] They consist of the MO_2 sheet of edge-sharing MO_6 octahedra. In the charge process, Na^+ is extracted between the neighboring MO_2 sheets and an electron is removed from the MO_2 sheet. In the discharge process, Na^+ is inserted between the neighboring MO_2 sheets and an electron is added to the MO_2 sheet. In order to develop high performance materials for SIB, deeper comprehension of the electronic state of TM is indispensable.

In this paper, we investigated the electronic structure of TM of four layered oxides ($Na_{0.91}CoO_2$, $Na_{0.66}CoO_2$, $Na_{1.00}MnO_2$, and $Na_{0.54}MnO_2$) by means of the HERFD-XANES with high energy resolution. As far as we know, there exists no report on application of the HERFD-XANES to TM in the battery materials. The high energy-resolved spectroscopy revealed a shoulder structure in the pre-edge regions of the Co K-edge spectra in $Na_{0.91}CoO_2$. The structure is ascribed to the transition to Co 3*d*/4*p* state via slight hybridization with the Na 3*s* state.

Layered oxides were prepared by solid state reaction. For $Na_{0.91}CoO_2$, Na_2O_2 and Co_3O_4 were mixed in a 1.25: 1 atomic ratio and calcined at 823 K for 16 h in O_2. Then, the product was finely ground, and again calcined in the same condition. For $Na_{0.66}CoO_2$, Na_2CO_3 and Co_3O_4 were mixed in a 0.7:1 atomic ratio and calcined at 1073 K for 12 h in air. For $Na_{1.00}MnO_2$, Na_2CO_3 and Mn_2O_3 were mixed in a 1: 1 atomic ratio and calcined at 943 K for 24 h in Ar. For $Na_{0.54}MnO_2$, Na_2CO_3 and $MnCO_3$ were mixed in a 0.7:1 atomic ratio and calcined at 1273 K for 12 h in air. The Na concentrations were determined by the Rietveld analyses of the synchrotron-radiation X-ray powder diffraction (XRD) patterns, as described below.

Synchrotron-radiation XRD measurements were performed at the BL-8A beamline of the Photon Factory, KEK. The samples were finely ground and placed in ϕ0.3 mm glass capillaries. The capillaries were sealed and mounted on the Debye-Scherrer camera. The powder diffraction patterns were detected with an imaging plate. The exposure time was 5 minutes. The wavelength (= 0.68903 Å) of the X-ray was calibrated by the lattice constant of standard CeO_2 powders. The XRD patterns of O3-$Na_{0.91}CoO_2$ was analyzed by the Rietveld method (Rietan-FP)[15] with a trigonal model ($R\bar{3}m$; Z = 3, hexagonal setting). The XRD pattern of the Mn-based O'3-$Na_{1.00}MnO_2$ was analyzed by the Rietveld method

with a monoclinic model ($C2/m$; Z = 2). The XRD patterns of the P2-$Na_{0.66}CoO_2$ and P2-$Na_{0.54}MnO_2$ were analyzed by the Rietveld method with a hexagonal model ($P6_3/mmc$; Z = 2). X-ray diffraction patterns and Rietveld refinement profiles are shown in Figs. S1 - S4. In all compounds, no traces of impurities nor secondary phases were observed. The obtained structural parameters are listed in Table S1 –S4.

The Co and Mn K-edge XANES spectra were measured in both the transmission and HERFD modes. The measurements of the transmission XANES were conducted at BL-9C beamline of the Photon Factory, KEK. The powder was finely ground, mixed with BN, and pressed into pellets with 5 mm in diameter. The transmission XANES were recorded with a Si (111) double-crystal monochromator at 300 K. The energy resolution ($\Delta E/E$) was ~2×10^{-4} and the photon flux at sample position was ~1×10^{11} phs/s. The measurements of the HERFD-XANES were carried out at the contract undulator beamline BL11XU of SPring-8.[16,17] The incident X-ray beam was monochromatized with a Si (111) double-crystal monochromator followed by a 2-bounce Si (400) channel-cut monochromator to further increase the incident energy resolution (263 meV at 7670 eV and ΔE = 288 meV at 6460 eV). The pellet sample was placed at normal incident angle (ϕ = 85°) and grazing exit angle (θ = 5°) to the surface in order to suppress the self-absorption.[18] The estimated contributions of self-absorption for the pre-edge regions at Co and Mn K-edges are less than 0.5% and therefore it is negligible. The estimated contributions of self-absorption for the main absorption peak at Co and Mn K-edges are less than 10%. The details of the estimation is described in Supplementary Data. The beam size at sample position was about 0.05 mm (horizontal) × 1 mm (vertical) and the photon flux was ~ 8×10^{12} phs/s. The emitted X-rays in the horizontal plane were analyzed by a Rowland-mount type emission spectrometer. To select the Co $K_{\beta_{1,3}}$ fluorescence line (~7650 eV), a Ge (444) spherically bent analyzer was used. The total energy resolution was ~1.2 eV at 7650 eV. To select the Mn $K_{\beta_{1,3}}$ fluorescence line (~6490 eV), a Si (333) spherically bent analyzer was used. The total energy resolution was ~1.2 eV at 6490 eV. In the analyses, the background subtraction and normalization were performed using the ATHENA program.[19]

The partial density of states (pDOSs) were calculated for O3-$NaCoO_2$ and O'3-$NaMnO_2$ based on the density functional theory with use of the plane-wave self-consistent field (PWscf) package.[20] A plane wave basis set with a cutoff energy of 952 eV was chosen,

and the projector-augmented wave (PAW) potentials were used. We adopted the exchange-correlation functional of Perdew-Burke-Ernzerhof type within generalized gradient approximation. Electron spin was taken into account in the level of local spin density approximation. In the calculation of O3-$NaCoO_2$, we used the lattice constant (*a* and *c*) and atomic coordinates of O3-$Na_{0.91}CoO_2$ obtained by the Rietvelt refinement (Table S1). In the calculation of O'3-$NaMnO_2$, we used the lattice constant (*a*, *b* and *c*) and the atomic coordinates of O3-$Na_{1.00}MnO_2$ obtained by the Rietvelt refinement (Table S3). Brillouin-zone sampling for the pDOS calculations was made using the Monkhorst-Pack method with 36 × 36 × 24 and 24 × 36 × 24 *k* points for O3-$NaCoO_2$ and O'3-$NaMnO_2$, respectively.

Figure 2 (a) shows the Co K-edge XANES spectra of $Na_{0.91}CoO_2$ recorded in the HERFD (red circle) and transmission (solid black line) modes. The main absorption peak observed at 7725 eV is ascribed to the electric dipole transition from Co 1*s* to Co 4*p* orbital. Although the peak-top intensity of Co K-edge HERFD-XANES spectrum is slightly higher than that of transmission spectra, the peak width is no significant spectral difference between the two modes, indicating the main peak has intrinsic line width wider than Γ_K (=1.33 eV). Importantly, we observed significant spectral difference in the pre-edge region [inset in Fig. 2(a)]. The HERFD-XANES spectrum shows a shoulder structure at around 7708 eV while no trace of the structure is discernible in the conventional transmission spectrum. Figure 2 (b) shows the Mn K-edge XANES spectra of $Na_{1.00}MnO_2$ recorded in the HERFD (red circle) and transmission (solid black line) modes. The main absorption peak observed at 6555 eV is ascribed to the electric dipole transition from Mn 1*s* to Mn 4*p* orbital. Although the peak-top intensity of Mn K-edge HERFD-XANES spectrum is slightly higher than that of transmission spectra, the peak width is no significant spectral difference between the two modes, indicating the main peak has intrinsic line width wider than Γ_K (=1.16 eV). In the pre-edge region (inset in Fig. 2(b)), however, we observed significant spectral difference between the two modes, reflecting higher energy resolution in the HERFD mode. The HERFD-XANES spectrum shows well-resolved two sharp absorptions at 6535 and 6537 eV. This makes a sharp contrast with the much broader structure in the transmission mode. Similarly, we observed extra fine pre-edge structures in the Co K-edge XANES spectrum of $Na_{0.66}CoO_2$ and Mn K-edge XANES spectrum of $Na_{0.54}MnO_2$ recorded in HERFD mode (Figure 5S).

In Fig. 3(a), we compare the Co K-edge HERFD-XANES spectra in the pre-edge region between $Na_{0.91}CoO_2$ and $Na_{0.66}CoO_2$. With increase in the formal valence of Co from +3.09 ($Na_{0.91}CoO_2$) to +3.34 ($Na_{0.66}CoO_2$), the intensity of the band at 7706 eV increases. The behavior is reasonable because $Na_{0.66}CoO_2$ has higher density of states in the unoccupied 3*d* orbitals. In Fig. 3(b), we compare the Mn K-edge HERFD-XANES spectra in the pre-edge region between $Na_{1.00}MnO_2$ and $Na_{0.54}MnO_2$. In both the spectra, well-resolved two absorption bands are observed at 6535eV and 6537eV. With increase in the formal valence of Mn from +3.00 ($Na_{1.00}MnO_2$) to +3.46 ($Na_{0.54}MnO_2$), the intensity of the higher-lying band at 6537eV increases. The behavior is reasonable because $Na_{0.54}MnO_2$ has higher density of states in the unoccupied 3*d* orbitals.

Let us compare the K-edge HERFD-XANES spectra in the pre-edge region with the first-principles calculations. Figure 4(a) shows Co (blue curves), O (red curves), and Na (green curves) pDOSs of O3-$NaCoO_2$. The system is a non-magnetic insulator with the gap of ~ 1 eV.[20] The O3-type structures consist of the CoO_2 sheet of the edge-sharing CoO_6 octahedra, causing crystal field splitting of the Co 3*d* orbital into the lower-lying t_{2g} and upper-lying e_g ones. The t_{2g} and e_g states correspond to the bands at around -0.8 and 1.6 eV, respectively. The t_{2g} band is fully occupied while the e_g band is unoccupied. We observed a strong O 2*p* – Co 3*d* hybridization in both the t_{2g} and e_g bands. The 7706 eV peak observed in the Co K-edge spectrum in the pre-edge region [Fig.3(a)] is assigned to the transition from the Co 1*s* to the e_g band. We note that rather broad Na 3s state is observed at higher energy region above 4eV. We calculated the integrated pDOdoSs in the Na 3*s* band from 3.5 to 6.0 eV (see Table 1). Even though the Na 3s band is dominated by the Na 3*s* and O 2*p* state, the band contains the Co 4*s* (l = 0), Co 3*d* (l = 1) and Co 4*p* (l= 2) states. This suggests that the Co 3*d*/4*s*/4*p* states is hybridized with Na 3*s* and O 2*p* state. We further confirmed that the errors of pDOSs were within 6.5% by *ab initio* calculation under three different conditions (Table S5). Since the Co 1*s* – Co 4*s* transition is forbidden, we ascribed the shoulder structure above 7708 eV to the transition to the Co 3*d*/4*p* states via slight hybridization with the Na 3*s* state. The shoulder structure seems to disappear in $Na_{0.66}CoO_2$. This is probably due to the energy difference between the up and down spin e_g bands, and resultant broadening of the XANES spectrum. Actually, *ab initio* calculation of P2-$Na_{1/2}CoO_2$[21] shows the energy difference of ~ 1 eV between the up and down spin e_g bands.

Figure 4(b) shows Mn (blue curves), O (red curves), and Na (green curves) pDOSs of O'3-$NaMnO_2$. The system is an antiferromagnetic insulator with the gap of ~ 1 eV. The total energy of the antiferromagnetic state is lower by 65 ± 2 meV/FU than that of the competing ferromagnetic state. The magnitude and direction of the Mn spin is 3.09 m_B and perpendicular to the MnO_2 layer, respectively. The electronic structure of $NaMnO_2$ is similar to that of isostructural $LiMnO_2$.[22] The O'3-type structures consist of the MnO_2 sheet of the edge-sharing MnO_6 octahedra with Jahn-Teller distortion, causing crystal field splitting of the Mn 3*d* orbital into the lower-lying t_{2g} and upper-lying e_g ones. The t_{2g} and e_g bands correspond to the bands around 1.0 and 2.4 eV, respectively. The fine structure in the t_{2g} bands is probably ascribed to the Jahn-Teller distortion. We observed strong O 2*p* – Co 3*d* hybridization in both the t_{2g} and e_g bands. The 6535eV and 6537eV peaks observed in the Mn K-edge spectrum in the pre-edge region [Fig.3(b)] are assigned to the transition from the Mn 1*s* to the t_{2g} and e_g bands, respectively. Similarly to the case of $Na_{0.91}CoO_2$, we may expect a shoulder structure due to the transition to the Mn 3*d*/4*p* states (see Table 2 and Table S6). Nevertheless, no trace of the structure is observed in $Na_{1.00}MnO_2$ and $Na_{0.54}MnO_2$. This is probably because lower-lying tail of the strong main absorption at 6555 eV obscures the structure.

Now, let us discuss the interrelation between the intrinsic linewidth and core-hole lifetime width (Γ_K and Γ_M). In both the Co and Mn compounds, the peak widths of the main absorption peaks that are dominated by the 1*s* – 4*p* transition show no significant difference between the two modes (Fig. 2, Table S7). In addition to the small contribution of self-absorption for the main absorption peak (less than 10%), this observation indicates that the intrinsic linewidths of the main peaks are wider than Γ_K. Probably, the main peak is overlapped by the transition to the continuum states such as 5*p*, 6*p*, and 7*p* to cause the wide linewidth. On the other hand, the spectral profiles due to the 1*s* – 3*d* transition in the pre-edge region show significant difference between the two modes. This observation indicates that the intrinsic linewidths of the 1*s* – 3*d* transitions are narrower than Γ_K. As explained in the introduction, the lifetime width of the HERFD-XANES (Γ) is mainly determined by Γ_M instead of Γ_K. Considering that 2*p*- core hole lifetime width Γ_L of Mn is ~0.5 eV,[5] the value of Γ_M ($< \Gamma_L$) is considered to be much smaller than 0.5 eV. For further quantitative argument, we should properly consider the instrumental resolution. In the HERFD-XANES at BL11XU beamline of SPring-8, the instrumental resolution (Γ_{inst}), which mainly originated in linewidth of the incident X-ray and the crystal analyzer, was

~1.2 eV at the Co and Mn $K_{\beta_{1,3}}$ fluorescence line. We note that Γ_{inst} is comparable to Γ_{K} of Co (= 1.33 eV) and Mn (= 1.16 eV). Then, the actual energy resolution of the HERFD-XANES is mainly governed by Γ_{inst} and is slightly larger than 1.2 eV. A future improvement of the spectrometer as well as the X-ray source would enhance the energy resolution.

In conclusions, we investigated the electronic structure of TM of four layered oxides ($Na_{0.91}CoO_2$, $Na_{0.66}CoO_2$, $Na_{1.00}MnO_2$, and $Na_{0.54}MnO_2$) by means of HERFD-XANES with high energy resolution. The high energy-resolved spectroscopy revealed a shoulder structure in the pre-edge regions of the Co K-edge spectra in $Na_{0.91}CoO_2$. The structure is ascribed to the transition to the Co 3*d*/4*p* state via slight hybridization with the Na 3*s* state. Our experiment demonstrated that the HERFD-XANES can clarify the fine structures in the pre-edge regions of the Co and Mn K-edge spectra. We believe that application of HERFD-XANES to the other TM battery materials will contribute to deeper comprehension of the variation of the electronic structure with the redox processes. We note that the HERFD-XANES, which uses hard X-ray with high transmittance in materials, is suitable for *in situ*/*operando* measurements under electrochemical control.

Acknowledgments

This work was supported by JSPS KAKENHI (Grant Number JP16K20940 and JP17H0113). A part of this work was performed under the Shared Use Program of the National Institutes for Quantum and Radiological Science and Technology (QST) Facilities (Proposal No. 2016B-H03 and 2017A-H04) supported by the QST Advanced Characterization Nanotechnology Platform as a program of "Nano-technology Platform" (project No. A-16-QS-0018 and No. A-17-QS-0004) of the Ministry of Education, Culture, Sports, Science and Technology (MEXT), Japan. The synchrotron radiation experiments of HERFD-XAFS were performed at the BL11XU of SPring-8 with the approval of Japan Synchrotron Radiation Research Institute (Proposal No. 2016B3563 and No. 2017A3584). The transmission mode XAFS measurements were performed at BL-9C under the approval of the Photon Factory Program Advisory Committee (Proposal No. 2016G043 and 2017G002) and the X-ray powder diffraction experiments were performed at BL-8A under the approval of the Photon Factory Program Advisory Committee (Proposal No. 2014G507). Part of the *ab initio* calculation was performed using the supercomputing resources at Cyberscience Center, Tohoku University.

References

1) M. Newville, Rev. Mineral. Geochemistry. **78,** 33 (2014).

2) Y Iwasawa, K Asakura, M Tada, *XAFS Techniques for Catalysts, Nanomaterials, and Surfaces* (Springer, Switzerland, 2017).

3) A.E. Russell, A. Rose, Chem. Rev. **104**, 4613 (2004).

4) Y.-T. Cui, Y. Harada, H. Niwa, T. Hatanaka, N. Nakamura, M. Ando, T. Yoshida, K. Ishii, D. Matsumura, H. Oji, H. Ofuchi, and M. Oshima, Sci. Rep. **7**, 1482 (2017).

5) P. Glatzel and U. Bergmann, Coord. Chem. Rev. **249**, 65 (2005).

6) M. Bauer, Phys. Chem. Chem. Phys. **16**, 13827 (2014).

7) M. O. Krause and J. H. Oliver, Natural widths of atomic K and L levels, J. Phys. Chem. Ref. Data **8**, 329 (1979).

8) F.M.F. de Groot, M.H. Krisch, J. Vogel, Phys. Rev. B **66**, 195112 (2002).

9) N. Yabuuchi, K. Kubota, M. Dahbi, S. Komaba, Chem. Rev. **114**, 11636 (2014).

10) J.W. Choi, D. Aurbach, Nat. Rev. Mater **1**, 16013 (2016).

11) D. Kundu, E. Talaie, V. Duffort, L.F. Nazar, Angew. Chem. Int. Ed. **54**, 3432 (2015).

12) J.-Y. Hwang, S.-T. Myung, Y.-K. Sun, Chem. Soc. Rev. **46**, 3529 (2017).

13) Y. Lei, X. Li, L. Liu, G. Ceder, Chem. Mater. **26**, 5288 (2014).

14) M.H. Han, E. Gonzalo, G. Singh, T. Rojo, Energy Environ. Sci. **8**, 81 (2015).

15) F. Izumi and K. Momma, J. Solid State Phemom. **130**, 15 (2007).

16) K. Ishii, T. Tohyama and J. Mizuki, J. Phys. Soc. Jpn. **82**, 021015 (2013).

17) K. Ishii, I. Jarrige, M. Yoshida, K. Ikeuchi, T. Inami, Y. Murakami, and J. Mizuki, J. Electron Spectros. Relat. Phenomena **188**, 127 (2013).

18) P. Pfalzer, J.P. Urbach, M. Klemm, S. Horn, M.L. Den Boer, A.I. Frenkel, and J.P. Kirkland, Phys. Rev. B **60**, 9335 (1999).

19) B. Ravel and M. Newwille, J. Synchrotron. Rad. **12**, 537 (2005).

20) P. Giannozzi, S. Baroni, N. Bonini, M. Calandra, R. Car, C. Cavazzoni, et al., J. Phys. Condens. Matter. **21**, 395502 (2009).

21) H. Niwa, K. Higashiyama, K. Amaha, W. Kobayashi, and Y. Moritomo, J. Power Sources **384**, 156 (2018).

22) D.J. Singh, Phys. Rev. B **55**, 309 (1997).

Table 1. Integrated pDOS in the Na 3*s* band from 3.5 to 6.0 eV for O3-$NaCoO_2$. *l* is the azimuthal quantum number. Errors are evaluated by *ab initio* calculations under four different conditions. (See Table S5).

element	Na	O	Co (*l*=0)	Co (*l*=1)	Co (*l*=2)
pDOS (state/FU)	0.3421	0.1749	0.0167	0.0005	0.0085
Error (%)	1.5	0.6	6.5	0.1	5.4

Table2. Integrated pDOS in the Na 3*s* band from 3.0 to 5.0 eV for O'3-$NaMnO_2$. *l* is the azimuthal quantum number. Errors are evaluated by *ab initio* calculations under four different conditions. (See Table S6).

element	Na	O	Mn (*l*=0)	Mn (*l*=1)	Mn (*l*=2)
pDOS (state/FU)	0.2448	0.1552	0.0392	0.0003	0.0340
Error (%)	3.4	0.9	7.1	1.7	2.8

Figure captions

Figure 1.

(a) X-ray absorption and fluorescence processes. The former and latter processes were used in the transmission XANES and HERFD-XANES, respectively. Γ_K and Γ_M are 1s-core hole and 3p-core hole lifetime widths, respectively. K_{β_1} is the transition from M_3- to K-shell. K_{β_3} is the transition from M_2- to K-shell. (b) Experimental setup for HERFD-XAFS. The detection photon energy of the scattered X-ray is fixed at an energy of $K_{\beta 1,3}$ fluorescence line, while the energy of incident X-ray is scanned over the absorption edge.

Figure 2

(a) Co K-edge XANES spectra of $Na_{0.91}CoO_2$ recorded in the HERFD (red circle) and transmission (black solid line) modes. The two spectra were normalized at 7749 eV. (b) Mn K-edge XANES spectra of $Na_{1.00}MnO_2$ recorded in the HERFD (red circle) and transmission (black solid line) modes. The two spectra were normalized at 6579 eV. The insets show magnified spectra around the pre-edge regions.

Figure 3

(a) Pre-edge region of Co K-edge XANES spectra for $Na_{0.91}CoO_2$ and $Na_{0.66}CoO_2$ recorded in the HERFD mode. (b) Pre-edge region of Mn K-edge XANES spectra for $Na_{1.00}MnO_2$ and $Na_{0.54}MnO_2$ recorded in the HERFD mode.

Figure 4.

Calculated partial density of states (pDOSs) of (a) O3-$NaCoO_2$ and (b) O'3-$NaMnO_2$. Insets show schematic structures of O3-$NaCoO_2$ and O'3-$NaMnO_2$. E_f is the Fermi level.

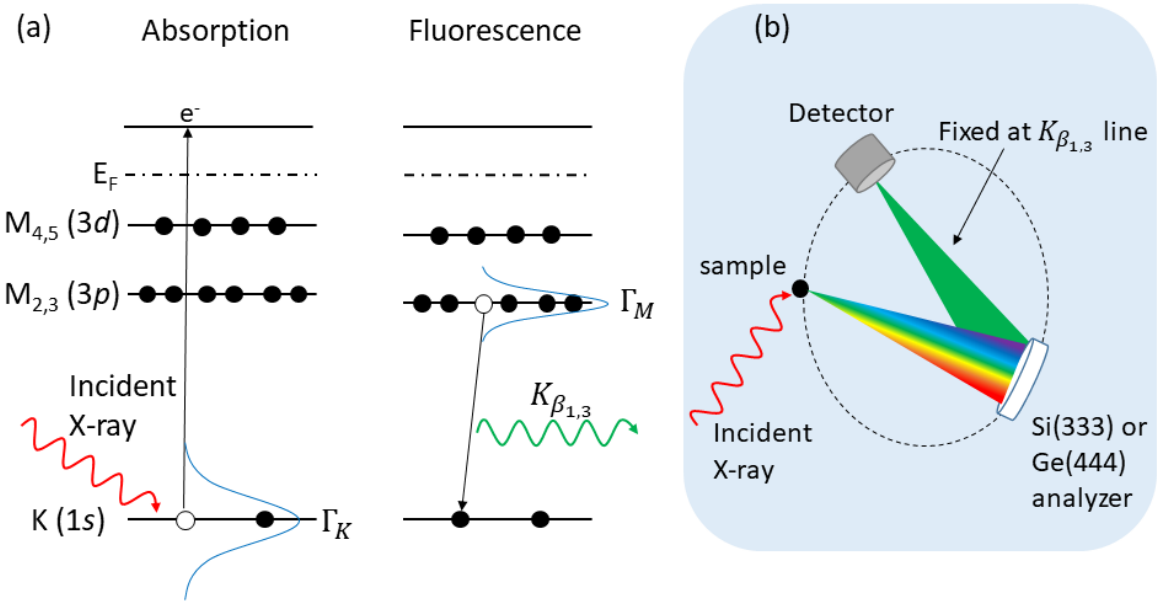
(a)
Absorption
Fluorescence
e⁻
E_F
M4,5 (3d)
M2,3 (3p)
Incident
X-ray
K (1s)
Γ_K
Γ_M
K_β1,3
(b)
Detector
Fixed at K_β1,3 line
sample
Incident
X-ray
Si(333) or
Ge(444)
analyzer

Figure 1

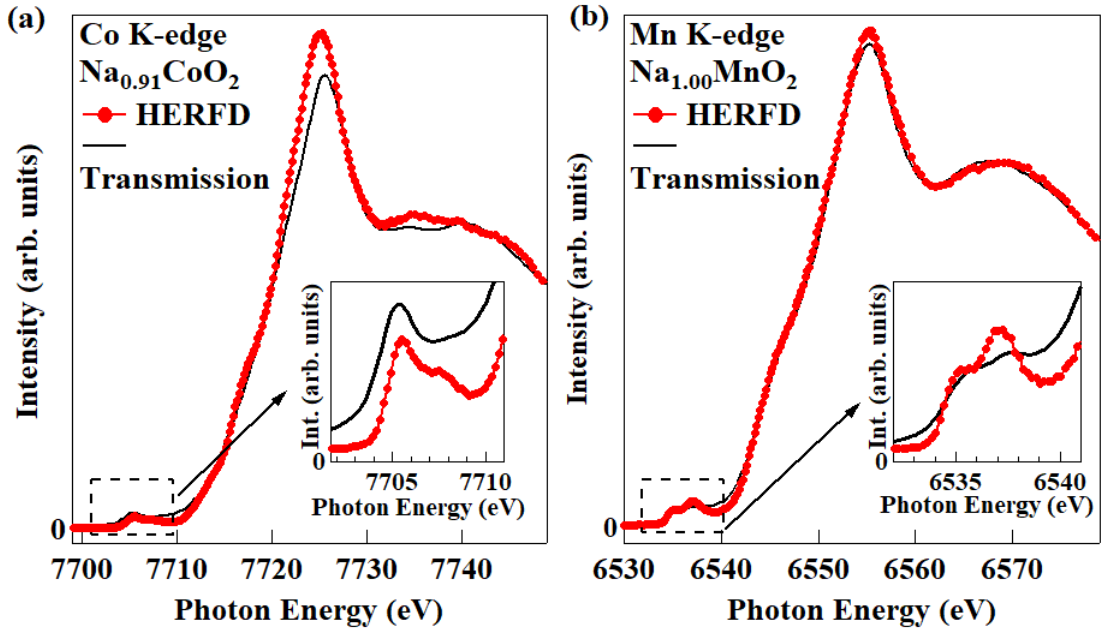
(a)
Co K-edge
$Na_{0.91}CoO_2$
HERFD
Transmission
Intensity (arb. units)
0
7700
7710
7720
7730
7740
Photon Energy (eV)
Int. (arb. units)
0
7705
7710
Photon Energy (eV)
(b)
Mn K-edge
$Na_{1.00}MnO_2$
HERFD
Transmission
Intensity (arb. units)
0
6530
6540
6550
6560
6570
Photon Energy (eV)
Int. (arb. units)
0
6535
6540
Photon Energy (eV)

Figure 2

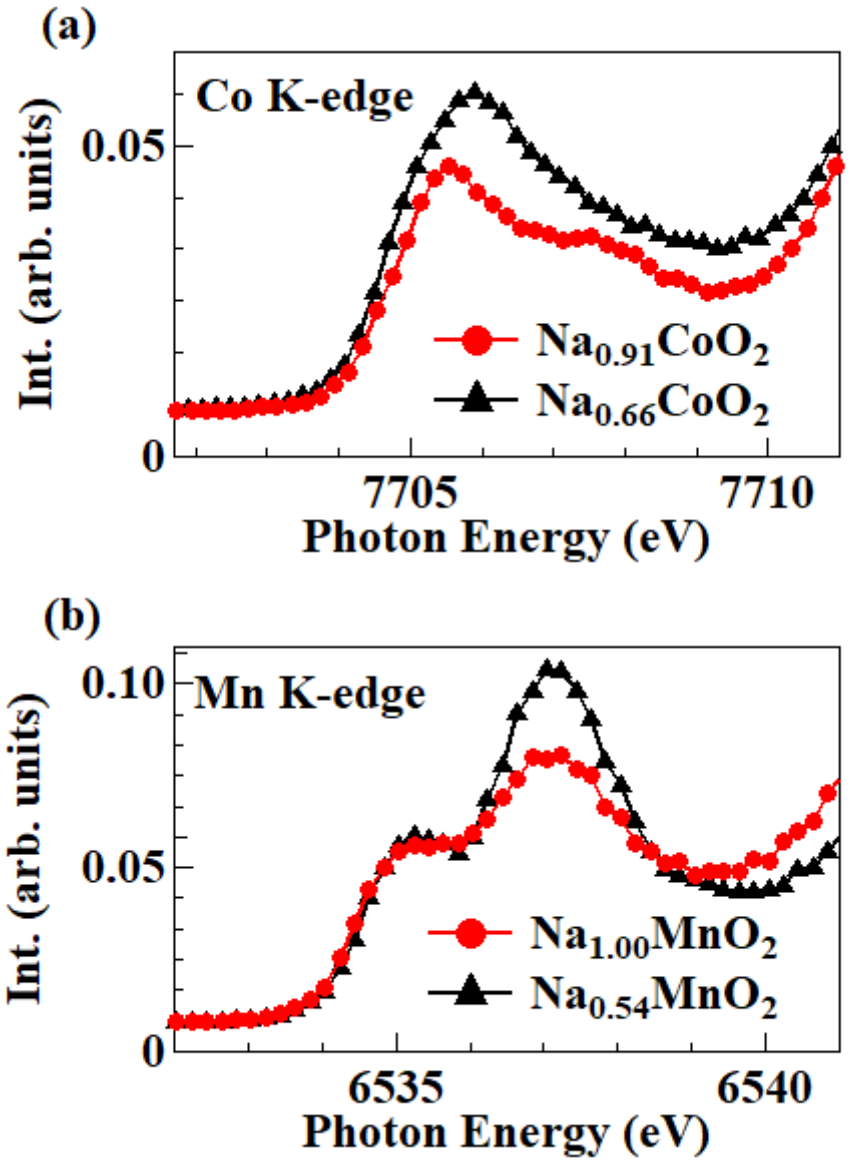
(a)
Co K-edge
Int. (arb. units)
0.05
0
7705
7710
Photon Energy (eV)
$Na_{0.91}CoO_2$
$Na_{0.66}CoO_2$
(b)
Mn K-edge
Int. (arb. units)
0.10
0.05
0
6535
6540
Photon Energy (eV)
$Na_{1.00}MnO_2$
$Na_{0.54}MnO_2$

Figure 3

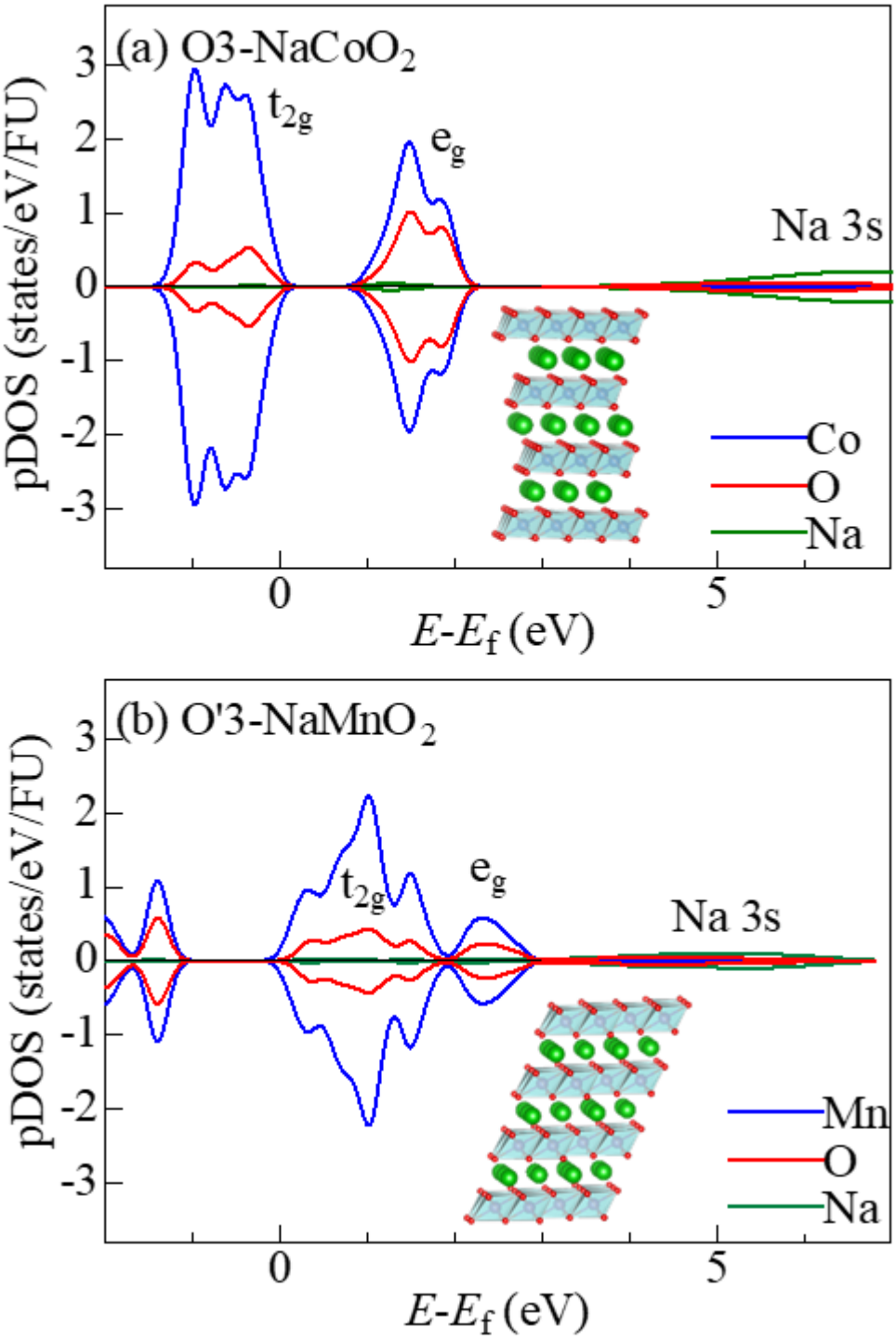
(a) O3-NaCoO2
t2g
eg
Na 3s
pDOS (states/eV/FU)
Co
O
Na
E-Ef (eV)
(b) O'3-NaMnO2
t2g
eg
Na 3s
pDOS (states/eV/FU)
Mn
O
Na
E-Ef (eV)

Figure4